

Article

Fault Current Characteristics of the DFIG under Asymmetrical Fault Conditions

Fan Xiao *, Zhe Zhang and Xianggen Yin

State Key Laboratory of Advanced Electromagnetic Engineering and Technology,
Huazhong University of Science and Technology, Wuhan 430074, China;
E-Mails: zz2012@163.com (Z.Z.); xianggeny@hust.edu.cn (X.Y.)

* Author to whom correspondence should be addressed; E-Mail: xiao103fan@163.com;
Tel.: +86-27-8754-0945.

Academic Editor: Frede Blaabjerg

Received: 20 July 2015 / Accepted: 16 September 2015 / Published: 30 September 2015

Abstract: During non-severe fault conditions, crowbar protection is not activated and the rotor windings of a doubly-fed induction generator (DFIG) are excited by the AC/DC/AC converter. Meanwhile, under asymmetrical fault conditions, the electrical variables oscillate at twice the grid frequency in synchronous dq frame. In the engineering practice, notch filters are usually used to extract the positive and negative sequence components. In these cases, the dynamic response of a rotor-side converter (RSC) and the notch filters have a large influence on the fault current characteristics of the DFIG. In this paper, the influence of the notch filters on the proportional integral (PI) parameters is discussed and the simplified calculation models of the rotor current are established. Then, the dynamic performance of the stator flux linkage under asymmetrical fault conditions is also analyzed. Based on this, the fault characteristics of the stator current under asymmetrical fault conditions are studied and the corresponding analytical expressions of the stator fault current are obtained. Finally, digital simulation results validate the analytical results. The research results are helpful to meet the requirements of a practical short-circuit calculation and the construction of a relaying protection system for the power grid with penetration of DFIGs.

Keywords: wind power; doubly-fed induction generator (DFIG); fault current characteristics; non-severe fault; asymmetrical fault

1. Introduction

Since wind energy is expected to play an important role in the future energy industry, wind power generation technology has received world-wide attention. Wind power generation based on the doubly-fed induction generator (DFIG) has gained increasing popularity due to several advantages, including smaller converter ratings around 30% of the generator rating, variable speed and four-quadrant active and reactive power operation capabilities, lower converter cost, and power losses compared with the fixed-speed induction generators or synchronous generators with full-sized converters [1,2]. As the power penetration from the DFIG-based wind turbines into the grid has increased steadily in recent years, the grid codes require that the wind power generators should not be tripped from the grid but stay connected during the fault conditions [3], which means that the wind turbines have the capability of low voltage ride through (LVRT) [4–6].

The operation characteristics of DFIG under LVRT conditions have a large influence on the fault characteristics of current [7]. This means that the DFIGs bring many new problems and challenges to the traditional relaying protection of the power grid. Therefore, in order to establish a solid basis for the relay protection study of the power grid with DFIGs, the fault current characteristics of the DFIG should be studied.

During severe fault conditions, in order to ensure the safety of the DFIG, the crowbar protection [8] will be activated to short circuit the rotor windings and divert the surge current from the rotor-side converter (RSC). Up to now, the fault current characteristics of the DFIG under severe fault conditions have been discussed widely [9–11]. Whereas the crowbar protection will not be activated and the rotor windings are still excited by the AC/DC/AC converter under non-severe fault conditions. The fault current characteristics of the DFIG under non-severe fault conditions, such as transient components and damping time constant, are much different from the severe fault conditions.

For non-severe fault conditions, the fault current of the DFIG is studied based on the assumption that the excitation current will keep constant before and after the fault occurrence [12] or rise rapidly to the maximum value and then keep constant during the grid faults [13]. However, since the response of the AC/DC/AC converter is very fast and complicated during the grid faults, the aforementioned assumptions do not seem to work. In [14,15], the dynamic behavior of the fault current of the DFIG under non-severe fault conditions has been discussed. Nevertheless, the research results are based on symmetric fault conditions, and there are no analytical expressions of the fault current under unbalanced fault conditions. Under unbalanced fault conditions, the conventional phase locked loop (PLL) techniques cannot present accurate phase angle estimation because the second harmonics produced by the negative-sequence component of the grid voltage will propagate through the PLL system and will be reflected in the extracted phase angle [16]. In the engineering practice, notch filters are usually used to extract the positive- and negative-sequence components [17,18]. This means that the transient behaviors of the DFIGs are changed by the notch filters and the research results presented in [14,15], do not agree with reality very well. Hence, further research works should be implemented to study the fault current characteristics of the DFIG under unbalanced fault conditions.

In order to fill this gap, a theoretical analysis method for the fault current characteristics of the DFIG under unbalanced fault conditions is proposed. Section 2 introduces the DFIG equations in space vector notation. Section 3 analyzes the influence of the notch filters on the proportional integral (PI)

parameters and the simplified calculation models of the rotor current are established. Section 4 analyzes the dynamic performance of the stator flux linkages. Based on this, the characteristics of the stator fault current under unbalanced fault conditions are studied in Section 5. Simulation results given in Section 6 validate the theoretical analysis results.

2. Doubly-Fed Induction Generator (DFIG) Equations in Space Vector Notation

The positive $(dq)^+$ and negative $(dq)^-$ synchronous rotating reference frames are chosen to model the DFIG based on the fifth-order two-axis representation, and the model of DFIG is commonly known as the “Park model” [19].

Using generator convention for the stator windings and motor convention for the rotor windings, the voltage equations and flux linkage equations are expressed as:

$$\begin{cases} u_{sd+}^+ = -R_s i_{sd+}^+ - \omega_1 \Psi_{sq+}^+ + p \Psi_{sd+}^+ \\ u_{sq+}^+ = -R_s i_{sq+}^+ + \omega_1 \Psi_{sd+}^+ + p \Psi_{sq+}^+ \\ u_{rd+}^+ = R_r i_{rd+}^+ - \omega_{r1} \Psi_{rq+}^+ + p \Psi_{rd+}^+ \\ u_{rq+}^+ = R_r i_{rq+}^+ + \omega_{r1} \Psi_{rd+}^+ + p \Psi_{rq+}^+ \end{cases} \quad (1)$$

$$\begin{cases} \Psi_{sd+}^+ = -L_s i_{sd+}^+ + L_m i_{rd+}^+ \\ \Psi_{sq+}^+ = -L_s i_{sq+}^+ + L_m i_{rq+}^+ \\ \Psi_{rd+}^+ = -L_m i_{sd+}^+ + L_r i_{rd+}^+ \\ \Psi_{rq+}^+ = -L_m i_{sq+}^+ + L_r i_{rq+}^+ \end{cases} \quad (2)$$

$$\begin{cases} u_{sd-}^- = -R_s i_{sd-}^- - \omega_2 \Psi_{sq-}^- + p \Psi_{sd-}^- \\ u_{sq-}^- = -R_s i_{sq-}^- + \omega_2 \Psi_{sd-}^- + p \Psi_{sq-}^- \\ u_{rd-}^- = R_r i_{rd-}^- - \omega_{r2} \Psi_{rq-}^- + p \Psi_{rd-}^- \\ u_{rq-}^- = R_r i_{rq-}^- + \omega_{r2} \Psi_{rd-}^- + p \Psi_{rq-}^- \end{cases} \quad (3)$$

$$\begin{cases} \Psi_{sd-}^- = -L_s i_{sd-}^- + L_m i_{rd-}^- \\ \Psi_{sq-}^- = -L_s i_{sq-}^- + L_m i_{rq-}^- \\ \Psi_{rd-}^- = -L_m i_{sd-}^- + L_r i_{rd-}^- \\ \Psi_{rq-}^- = -L_m i_{sq-}^- + L_r i_{rq-}^- \end{cases} \quad (4)$$

where u is the voltage, i is the current, R is the resistance, L is the inductance, and ψ is the flux linkage. The subscript d and q indicate the direct and quadrature axis components of the corresponding electrical quantity. The subscript s and r indicate the stator and rotor quantities, respectively. L_m is the magnetizing inductance. ω_1 is the synchronous angular velocity, and $\omega_2 = -\omega_1$. $\omega_{r1} = (\omega_1 - \omega_r)$ is the rotor slip in the positive dq frame, and $\omega_{r2} = (\omega_2 - \omega_r)$. The subscript “+” and “-” indicate positive-sequence and negative-sequence components, respectively. The superscript “+” and “-” indicate positive $(dq)^+$ and negative $(dq)^-$ synchronous rotating reference frames, respectively. $p = d/dt$ is the differential operator. Figure 1 depicts the equivalent circuit model of the DFIG.

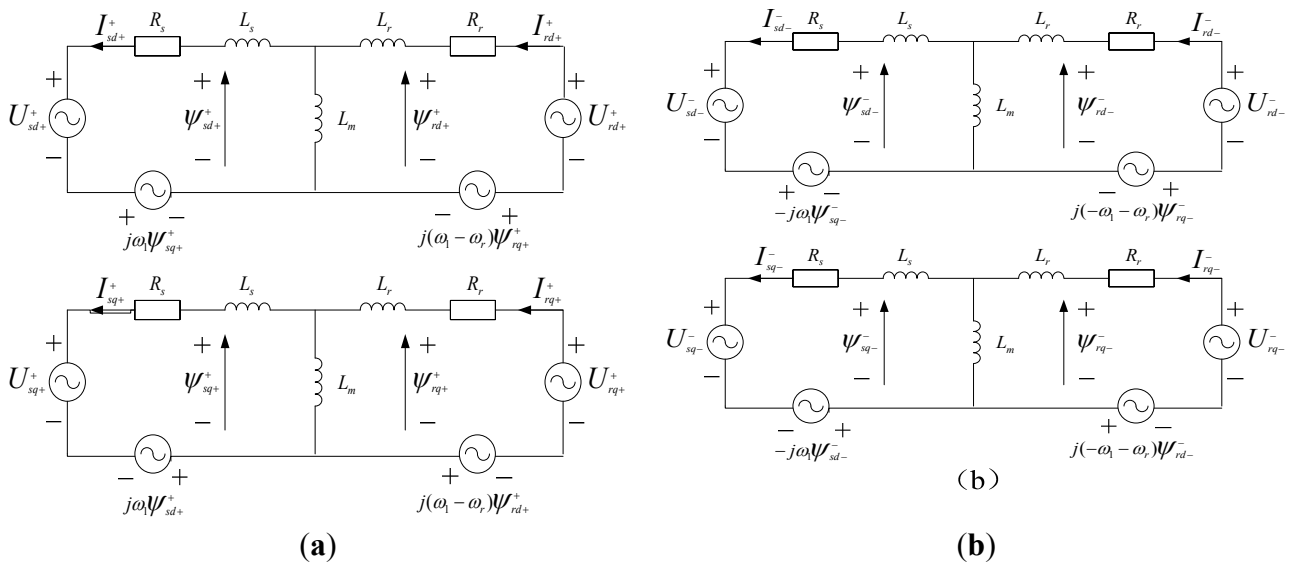


Figure 1. Equivalent circuit model of the doubly-fed induction generator (DFIG). (a) Equivalent circuit model of the DFIG in the positive dq reference frame rotating at the synchronous speed ω_1 ; and (b) equivalent circuit model of the DFIG in the negative dq reference frame rotating at the synchronous speed ω_2 .

3. Dynamic Behavior of the Rotor Current

During the fault transient period, the measurements of the active and reactive power are inaccurate. Moreover, it is unreasonable to make the DFIG operate with a unity power factor and capture the maximum wind power. Therefore, a typical handling method is to shut down the external power control loop when a fault is detected [20]. Under this condition, only the operation characteristics of the inner rotor current control loop are taken into consideration for the fault transient analysis. In addition, the rotation speed is considered constant for the following analysis.

3.1. Modeling of the Rotor-Side Converter (RSC)

According to the equations of Equations (2) and (4), the d -axis and q -axis components of the rotor flux linkages in $(dq)^+$ and $(dq)^-$ reference frames can be expressed in Equation (5) based on the stator flux linkages and the rotor currents:

$$\begin{cases} \psi_{rd+}^+ = -L_m(L_m i_{rd+}^+ - \psi_{sd+}^+) / L_s + L_r i_{rd+}^+ \\ \psi_{rq+}^+ = -L_m(L_m i_{rq+}^+ - \psi_{sq+}^+) / L_s + L_r i_{rq+}^+ \\ \psi_{rd-}^- = -L_m(L_m i_{rd-}^- - \psi_{sd-}^-) / L_s + L_r i_{rd-}^- \\ \psi_{rq-}^- = -L_m(L_m i_{rq-}^- - \psi_{sq-}^-) / L_s + L_r i_{rq-}^- \end{cases} \quad (5)$$

Meanwhile, the stator resistance is so small that it can be neglected. Under this condition, substituting Equation (5) and the first two equations of Equations (1) and (3) into the last two equations of Equations (1) and (3), the d -axis and q -axis components of the rotor voltage in $(dq)^+$ and $(dq)^-$ reference frames can be expressed:

$$\begin{cases} u_{rd+}^+ = (R_r i_{rd+}^+ + \sigma L_r p i_{rd+}^+) - \sigma \omega_{r1} L_r i_{rq+}^+ + (\omega_{slip1} \Psi_{sq+}^+ + U_{s+}) L_m / L_s \\ u_{rq+}^+ = (R_r i_{rq+}^+ + \sigma L_r p i_{rq+}^+) + \sigma \omega_{r1} L_r i_{rd+}^+ - \omega_{slip1} \Psi_{sd+}^+ L_m / L_s \\ u_{rd-}^- = (R_r i_{rd-}^- + \sigma L_r p i_{rd-}^-) - \sigma \omega_{r2} L_r i_{rq-}^- + (\omega_{slip2} \Psi_{sq-}^- + U_{s-}) L_m / L_s \\ u_{rq-}^- = (R_r i_{rq-}^- + \sigma L_r p i_{rq-}^-) + \sigma \omega_{r2} L_r i_{rd-}^- - \omega_{slip2} \Psi_{sd-}^- L_m / L_s \end{cases} \quad (6)$$

where $\sigma = 1 - L_m^2 / L_s L_r$, $\omega_{slip1} = \omega_1 - \omega_{r1}$, and $\omega_{slip2} = \omega_2 - \omega_{r2}$.

It can be seen from Equation (6) that the d -axis and the q -axis rotor voltages in $(dq)^+$ and $(dq)^-$ reference frames exert an effect on each other. Hence, in order to decouple the coupling terms $\sigma \omega_{r1} L_r i_{rq+}^+$, $\sigma \omega_{r1} L_r i_{rd+}^+$, $\sigma \omega_{r2} L_r i_{rq-}^-$, and $\sigma \omega_{r2} L_r i_{rd-}^-$ in both transient and steady-state conditions, the d -axis and the q -axis rotor currents can be separately controlled using feed forward compensation [21]. Moreover, it can be found from (6) that the tracking error of the rotor current is caused by the stator current and stator flux. Hence, the influence the terms $\omega_{r1} U_{s+} L_m / L_s$ and $\omega_{r2} U_{s-} L_m / L_s$ are done by the feed forward compensation and neglecting the derivative of the stator flux linkages.

In addition, due to the negative components oscillating at twice the grid frequency ($2\omega_1$) in the synchronous dq frame while the positive components are realized as DC quantities. Therefore, notch filters $N(s)$ are usually applied to filter out the influence of the 100-Hz frequency components, its structure is designed as:

$$N(s) = \frac{s^2 + \omega_n^2}{s^2 + 2\varepsilon\omega_n s + \omega_n^2} \quad (7)$$

where ω_n is the notch frequency which is the same as that of $2\omega_1$, and $\varepsilon\omega_1$ is the cutoff frequency of the notch filter.

Hence, under unbalanced fault conditions, the notch filters are applied to filter out the influence of the 100-Hz frequency component of the d -axis and q -axis components of the rotor currents in $(dq)^+$ and $(dq)^-$ reference frames. Moreover, the time delay of the pulse-width modulation (PWM) control is disregarded because PWM control has a speed that is markedly faster than that of the electromagnetic dynamic [20]. Hence, taking the control diagram of d -axis and q -axis component in the $(dq)^+$ reference frame, for example, the simplified block diagram of the rotor current control loop of the RSC is shown in Figure 2. In Figure 2, $G_{PI1}(s)$ is the transfer function of the PI₁ controller. The u_{rd+}^+ , u_{rq+}^+ , u_{rd-}^- , and u_{rq-}^- are controlled by the errors of the rotor current.

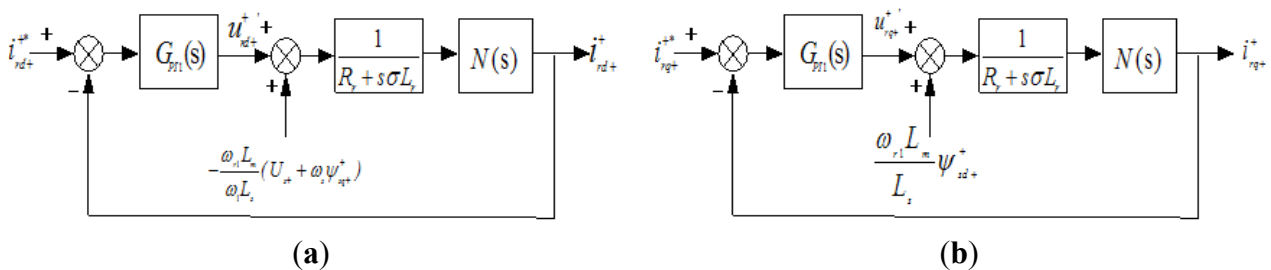


Figure 2. Simplified block diagram of the inner rotor current control loop of the RSC: (a) simplified control diagram of the d -axis component in $(dq)^+$ reference frame; and (b) simplified control diagram of the q -axis component in $(dq)^+$ reference frame. RSC: rotor-side converter.

In Figure 2, both the rotor current references and the stator flux linkages influence the dynamic response characteristics of the rotor current. In fact, the dynamic response characteristics of the rotor current are essentially a function of stator voltage because the inputs of the stator flux linkages are determined by the voltage.

The rotor voltage references are used to generate the PWM wave to control RSC switching. Hence, the rotor voltages of the DFIG can be expressed in Equation (8):

$$\begin{cases} u_{rd+}^+ = u_{rd+}^{+*} - \sigma\omega_{r1} L_r i_{rq+}^+ + U_{s+} L_m / L_s \\ u_{rq+}^+ = u_{rq+}^{+*} + \sigma\omega_{r1} L_r i_{rd+}^+ \\ u_{rd-}^- = u_{rd-}^{-*} - \sigma\omega_{r2} L_r i_{rq-}^- + U_{s-} L_m / L_s \\ u_{rq-}^- = u_{rq-}^{-*} + \sigma\omega_{r2} L_r i_{rd-}^- \end{cases} \quad (8)$$

Assuming that the rotor voltages can always track the references by space vector pulse width modulation, the rotor voltage references are obtained by:

$$\begin{cases} u_{rd+}^{+*} = k_{irp+} (i_{rd+}^{+*} - i_{rd+}^+) + k_{iri+} \int (i_{rd+}^{+*} - i_{rd+}^+) dt \\ u_{rq+}^{+*} = k_{irp+} (i_{rq+}^{+*} - i_{rq+}^+) + k_{iri+} \int (i_{rq+}^{+*} - i_{rq+}^+) dt \\ u_{rd-}^{-*} = k_{irp-} (i_{rd-}^{-*} - i_{rd-}^-) + k_{iri-} \int (i_{rd-}^{-*} - i_{rd-}^-) dt \\ u_{rq-}^{-*} = k_{irp-} (i_{rq-}^{-*} - i_{rq-}^-) + k_{iri-} \int (i_{rq-}^{-*} - i_{rq-}^-) dt \end{cases} \quad (9)$$

where k_{irp+} and k_{iri+} are the proportional and integral constants of the inner controller in the $(dq)^+$ reference frame, respectively. k_{irp-} and k_{iri-} are the proportional and integral constants of the inner controller in $(dq)^-$ reference frame, respectively. The i_{rd+}^{+*} and i_{rq+}^{+*} are the reference signals of the d -axis and q -axis components of the rotor current in $(dq)^+$ reference frame, respectively. The i_{rd-}^{-*} and i_{rq-}^{-*} are the reference signals of the d -axis and q -axis components of the rotor current in $(dq)^-$ reference frame, respectively.

3.2. Range of the Crossover Frequency and Phase Margin

It can be seen from the Figure 2, the open-loop transfer function of the control system without time delay can be presented as:

$$G_{pi}(s)G_r(s)N(s) = (k_{irp+} + \frac{k_{iri+}}{s}) (\frac{1}{R_r + s\sigma L_r}) (\frac{s^2 + \omega_n^2}{s^2 + 2\varepsilon\omega_n s + \omega_n^2}) \quad (10)$$

where $G_r(s)$ is the transfer function of a DFIG’s motor body.

Assume that the reference signals of the expected phase margin and expected crossover frequency are, respectively, ω_{cr}^* and ϕ_m^* . According to the control theory, the magnitude response of the open-loop transfer function at the crossover frequency ω_{cr}^* should be 0 dB; thus, the following equation can be established as:

$$\begin{aligned} & |G_{pi}(j\omega_{cr}^*)G_r(j\omega_{cr}^*)N(j\omega_{cr}^*)| \\ &= \frac{\sqrt{k_{irp+}^2 \omega_{cr}^{*2} + k_{iri+}^2}}{\omega_{cr}^*} \cdot \frac{1}{\sqrt{R_r^2 + (\omega_{cr}^* \sigma L_r)^2}} \cdot \frac{|\omega_n^2 - \omega_{cr}^{*2}|}{\sqrt{(\omega_n^2 - \omega_{cr}^{*2})^2 + (2\varepsilon\omega_n \omega_{cr}^*)^2}} = 1 \end{aligned} \quad (11)$$

The phase angle of this forward path loop gain at the cross over frequency ω_{cr}^* is given, in radians, by:

$$\begin{aligned} \angle\{G_{pi}(j\omega_{cr}^*)G_r(j\omega_{cr}^*)N(j\omega_{cr}^*)\} &= -\pi + \phi_m^* \\ &= \angle\left\{\left(k_{irp+} + \frac{k_{iri+}}{j\omega_{cr}^*}\right)\left(\frac{1}{R_r + j\omega_{cr}^*\sigma L_r}\right)\left(\frac{\omega_n^2 - \omega_{cr}^{*2}}{\omega_n^2 - \omega_{cr}^{*2} + j\omega_{cr}^* \cdot 2\varepsilon\omega_n}\right)\right\} \\ &= \arctan\frac{\omega_{cr}^*k_{irp+}}{k_{iri+}} - \frac{\pi}{2} - \arctan\frac{\sigma L_r \omega_{cr}^*}{R_r} - \arctan\frac{2\varepsilon\omega_n \omega_{cr}^*}{\omega_n^2 - \omega_{cr}^{*2}} \end{aligned} \tag{12}$$

According to Equations (11) and (12), the following controller parameters are found:

$$\begin{cases} k_{irp+} = AB/\omega_{cr}^* \sqrt{1 + A^2} \\ k_{iri+} = B/\sqrt{1 + A^2} \end{cases} \tag{13}$$

with $A = \tan[\phi_m^* + \arctan(\sigma L_r \omega_{cr}^*/R_r) + \arctan 2\varepsilon\omega_n \omega_{cr}^*/(\omega_n^2 - \omega_{cr}^{*2}) - \pi/2]$ and $B = \omega_{cr}^* \sqrt{(\sigma L_r \omega_{cr}^*)^2 + R_r^2} \cdot \sqrt{(\omega_n^2 - \omega_{cr}^{*2})^2 + (2\varepsilon\omega_n \omega_{cr}^*)^2} / |\omega_n^2 - \omega_{cr}^{*2}|$.

In order to ensure the ability to rapidly change the signal of the current loop and reduce the signal distortion, the bandwidth ω_{cb} of the closed loop system will take more than the maximum frequency ω_{cmax} of the effective signal. Moreover, in order to avoid the effect of the switching harmonics, the switching harmonics want to exist in the high frequency band of the inner rotor current control loop. Hence, the switching frequency should be higher than $10\omega_{cb}$.

In engineering, the desired closed-loop bandwidth of the inner rotor current control loop is usually takes values between 1.1 and 1.4 times of the crossover frequency of open loop system [22]. Accordingly, the range of the expected crossover frequency ω_{cr}^* in the closed loop system can be obtained:

$$\omega_{cmax}/k < \omega_{cr}^* \leq \frac{2\pi}{10k} \cdot \frac{1}{T_s} \text{ and } k \in (1.1, 1.4) \tag{14}$$

where $\omega_{cmax} = 2\pi p n_{max}/60$ and T_s is the control period of the rotor inverter. p is the number of pole pairs and n_{max} is the maximum speed of the rotor.

From Equation (11), the phase margin can be obtained as shown in Equation (15) if the controller time constant is designed as $k_{irp+}/k_{iri+} = \sigma L_r/R_r$:

$$\phi_m = \frac{\pi}{2} - \arctan\frac{2\varepsilon\omega_n \omega_{cr}^*}{\omega_n^2 - \omega_{cr}^{*2}} \tag{15}$$

When the phase margin is higher than the value of ϕ_m in Equation (15), the effect of the integrating element will drop steeply and steady tracking performance will be worsened. Therefore, the value of ϕ_m in Equation (15), is set as the maximum phase margin of the PI controller in the engineering application. Accordingly, the range of the expected phase margin ϕ_m^* can be obtained:

$$\phi_m^* \leq \frac{\pi}{2} - \arctan\frac{2\varepsilon\omega_n \omega_{cr}^*}{\omega_n^2 - \omega_{cr}^{*2}} \tag{16}$$

3.3. Transient Characteristics of Rotor-Side Converter (RSC)

According to the Figure 2a, the d -axis component of the rotor current in $(dq)^+$ reference frame is:

$$i_{rd+}^*(s) = G_{ird1+}^*(s)i_{rd+}^{*+}(s) - G_{ird2+}^*(s)p\Psi_{sd+}^*(s) \tag{17}$$

where:

$$G_{ind1+}^+(s) = \frac{G_{PI1}(s)N(s)}{R_r + s\sigma L_r + G_{PI1}(s)N(s)} \tag{18}$$

and:

$$G_{ind2+}^+(s) = \frac{N(s)}{R_r + s\sigma L_r + G_{PI1}(s)N(s)} \tag{19}$$

In order to get the maximum phase margin for the inner rotor current controller, substitute $k_{ip+}/k_{ir+} = \sigma L_r/R_r$ into Equation (13) to obtain the expressions of k_{ir+} as given in Equation (20):

$$k_{ir+} = R_r \omega_c^* \sqrt{(\omega_n^2 - \omega_{cr}^{*2}) + (2\varepsilon \omega_n \omega_{cr}^*)^2} / (\omega_{cr}^{*2} - \omega_n^2) \tag{20}$$

According to the range of the expected crossover frequency ω_{cr}^* in Equation (14), the range of the integral constant k_{ir+} can be obtained:

$$4.1 \cdot \omega_n R_r < k_{ir+} \leq 8.06 \cdot \omega_n R_r \tag{21}$$

with $\omega_n R_r \approx 1.063$.

According to the range of the integral constant k_{ir+} , substitute $k_{ip+}/k_{ir+} = \sigma L_r/R_r$ into Equation (10), the root locus diagram of the open-loop transfer function is shown in Figure 3.

From Figure 3, it can be observed that the eigenvalues of the system are located in the left-half-plane which means that the control system is stable. Moreover, it can be observed that the range of the imaginary part for the dominant pole is between 610 and 640. This means that the response component of the dominant poles of the system will be limited by the notch filters. Hence, $G_{ind1+}^+(s) \approx 1$.

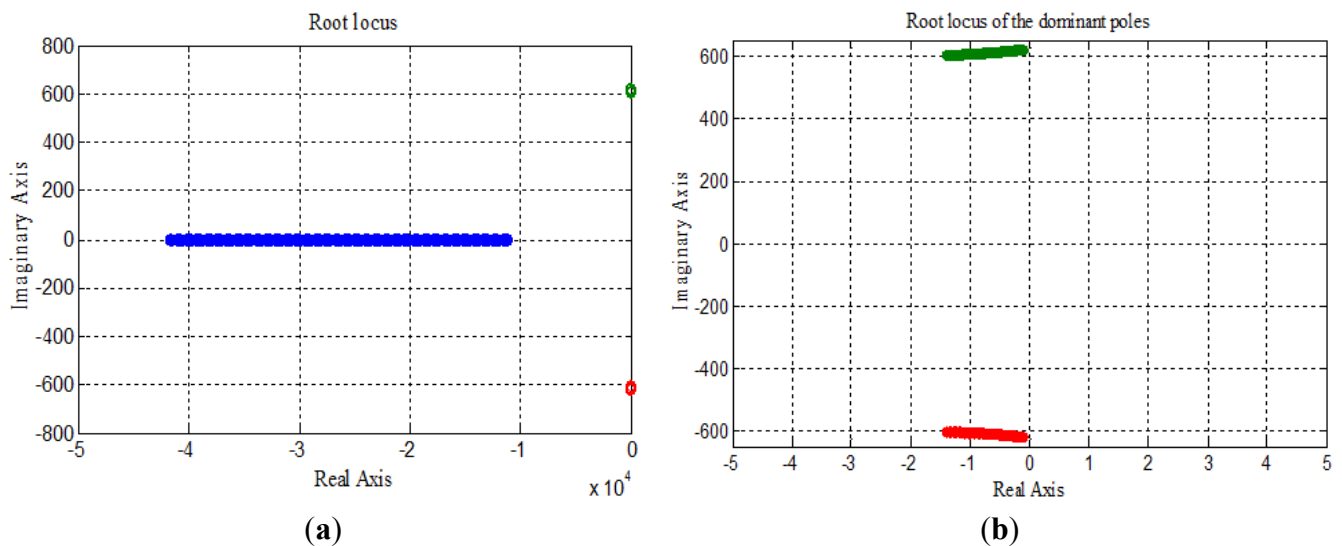


Figure 3. Root locus diagram of the open-loop transfer function. (a) root locus with a changing ω_{cr}^* ; and (b) the dominant poles of the of the open-loop transfer function with a changing ω_{cr}^* .

Accordingly, by substituting Equation (7) and $k_{ip+}/k_{ir+} = \sigma L_r/R_r$ in the equation of Equation (19), the closed-loop transfer function to the disturbance of differential flux during the fault transient period is:

$$G_{ind2+}^+(s) = \frac{s^3 + \omega_n^2 s}{(R_r + s\sigma L_r)[s^3 + (2\varepsilon \omega_n + k_{ir+}/R_r)s^2 + \omega_n^2 s + k_{ir+} \omega_n^2/R_r]} \tag{22}$$

The bode diagram of $G_{ird2+}^+(s)$ is shown in Figure 4.

From Figure 4, it can be observed that the maximum gain of the closed loop transfer function to the disturbance component at $\omega = \omega_1$ is nearly -54.9 dB, which means that the harmonic component in $p\Delta\varphi_{sd}$ will be greatly damped. Hence:

$$i_{rd+2}^+ = G_{ird2+}^+(s)p\psi_{sd+}^+ \approx 0 \tag{23}$$

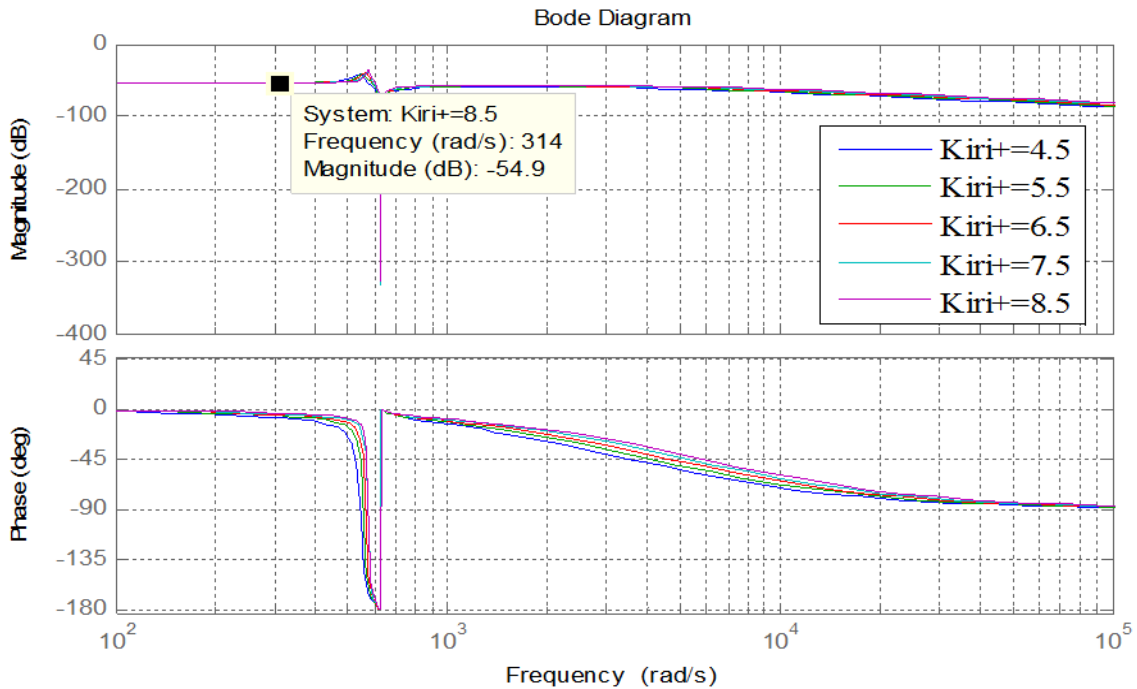


Figure 4. Bode diagram of the inner current closed-loop transfer function to the disturbance component (such as $p\psi_{sd+}^+$) during the fault transient period.

Hence, during the fault transient period, the d -axis and q -axis component of the rotor current in $(dq)^+$ reference frame are:

$$\begin{cases} i_{rd+}^+ \approx i_{rd+}^{+*} \\ i_{rq+}^+ \approx i_{rq+}^{+*} \end{cases} \tag{24}$$

According to the [23], the total reference of rotor current results from the addition of two terms. The first term is the reference signal of steady-state components i_{rj}^* . The second term is the demagnetizing current that helps to reduce or eliminate the electromotive force induced in the rotor. It is calculated from the natural flux i_m^* . Hence, the reference signal of the rotor current in $(dq)^+$ reference frame can be expressed:

$$\begin{cases} i_{rd+}^{+*} = i_{rd+}^{+*} + i_{rdn+}^{+*} = i_{rd+}^{+*} - K_d \cdot \psi_{sdn+}^+ \\ i_{rq+}^{+*} = i_{rq+}^{+*} + i_{rqn+}^{+*} = i_{rq+}^{+*} - K_d \cdot \psi_{sqn+}^+ \end{cases} \tag{25}$$

with $K_d = L_m / (\sigma L_s L_r)$. ψ_{sdn+}^+ and ψ_{sqn+}^+ are the natural components of the stator flux in the $(dq)^+$ reference frame, respectively.

Likewise, the expression as shown in Equation (26) can be obtained:

$$\begin{cases} \bar{i}_{rd-}^- \approx \bar{i}_{rd-}^{*-} = \bar{i}_{rd-}^{*-} + \bar{i}_{rdn-}^{*-} = \bar{i}_{rd-}^{*-} - K_d \cdot \Psi_{sdn-}^- \\ \bar{i}_{rq-}^- \approx \bar{i}_{rq-}^{*-} = \bar{i}_{rq-}^{*-} + \bar{i}_{rqn-}^{*-} = \bar{i}_{rq-}^{*-} - K_d \cdot \Psi_{sqn-}^- \end{cases} \quad (26)$$

where Ψ_{sdn-}^- and Ψ_{sqn-}^- are the natural components of the stator flux in the $(dq)^-$ reference frame, respectively.

4. Dynamic Performance of Stator Flux Linkage

According to the symmetrical component theory, if the grid supply is unbalanced, any three-phase quantity, e.g., voltage, current, or flux, denoted as a vector U_s can be separated into the positive and negative sequence components as:

$$U_s = U_{s+} e^{j\omega_1 t} + U_{s-} e^{-j\omega_1 t} \quad (27)$$

where U_{s+} and U_{s-} are the positive- and negative-sequence voltage components in the stator, respectively.

The notch filters $N(s)$ are applied to filter out the influence of the 100-Hz frequency component in the stator voltage in the $(dq)^+$ and $(dq)^-$ reference frames. Meanwhile, assuming that the d -axis of the reference frame is aligned with the stator voltage vector [24] and applying Laplace transformations to them, it can be obtained:

$$\begin{cases} u_{sd+}^+(s) = N(s)U_{s+}(s) + U_{s-}(s)N(s)/(s^2 + \omega_n^2), & u_{sq+}^+(s) = 0 \\ u_{sd-}^-(s) = N(s)U_{s-}(s) + U_{s+}(s)N(s)/(s^2 + \omega_n^2), & u_{sq-}^-(s) = 0 \end{cases} \quad (28)$$

By substituting Equations (25) and (26) into the first two Equations of (2) and (4), the d -axis and q -axis components of the stator currents can be expressed in Equation (29):

$$\begin{cases} \bar{i}_{sd+}^+(s) = L_m \bar{i}_{rd+}^{*+}(s)/L_s - [L_m K_d \Psi_{sdn+}^+(s) + \Psi_{sd+}^+(s)]/L_s \\ \bar{i}_{sq+}^+(s) = L_m \bar{i}_{rq+}^{*+}(s)/L_s - [L_m K_d \Psi_{sqn+}^+(s) + \Psi_{sq+}^+(s)]/L_s \\ \bar{i}_{sd-}^-(s) = L_m \bar{i}_{rd-}^{*-}(s)/L_s - [L_m K_d \Psi_{sdn-}^-(s) + \Psi_{sd-}^-(s)]/L_s \\ \bar{i}_{sq-}^-(s) = L_m \bar{i}_{rq-}^{*-}(s)/L_s - [L_m K_d \Psi_{sqn-}^-(s) + \Psi_{sq-}^-(s)]/L_s \end{cases} \quad (29)$$

Under stable operating conditions, the stator flux linkages can be obtained from the Equations (1) and (3) such that $\Psi_{sq+}^+ \approx -U_{s+}/\omega_1$, $\Psi_{sq-}^- \approx U_{s-}/\omega_1$, and $\Psi_{sd+}^+ = \Psi_{sd-}^- \approx 0$. Hence, the expressions of the natural flux can be obtained as:

$$\begin{cases} \Psi_{sdn+}^+ = \Psi_{sd+}^+ \\ \Psi_{sqn+}^+ = \Psi_{sq+}^+ + U_{s+}/\omega_1 \\ \Psi_{sdn-}^- = \Psi_{sd-}^- \\ \Psi_{sqn-}^- = \Psi_{sq-}^- - U_{s+}/\omega_1 \end{cases} \quad (30)$$

In fact, the response of the inner rotor current control loop is much faster than the dynamic change of the stator flux linkage [25]. Therefore, the terms $R_s L_m \bar{i}_{rd+}^{*+}$, $R_s L_m \bar{i}_{rq+}^{*+}$, $R_s L_m \bar{i}_{rd-}^{*-}$, and $R_s L_m \bar{i}_{rq-}^{*-}$ can be neglected. Moreover, the amplitude of the terms $R_s L_m K_d U_{s+}/\omega_1 L_s$ and $R_s L_m K_d U_{s-}/\omega_1 L_s$ are much smaller than U_{s+}/ω_1 and U_{s-}/ω_1 , respectively. Hence, the terms $R_s L_m K_d U_{s+}/\omega_1 L_s$ and $R_s L_m K_d U_{s-}/\omega_1 L_s$ can also be neglected. Based on this, substitute Equations (29) and (30) into the first two Equations of (1) and (3) and the voltage equations of the stator can be obtained as follows:

$$\begin{cases} u_{sd+}^+(s) = R_s \Psi_{sd+}^+(s)/L_s' - \omega_1 \Psi_{sq+}^+(s) + s \Psi_{sd+}^+(s) \\ 0 = R_s \Psi_{sq+}^+(s)/L_s' + \omega_1 \Psi_{sd+}^+(s) + s \Psi_{sq+}^+(s) + U_{sn}/\omega_1 \end{cases} \quad (31)$$

$$\begin{cases} u_{sd-}^- (s) = R_s \psi_{sd-}^- (s) / L'_s - \omega_2 \psi_{sq-}^- (s) + s \psi_{sd-}^- (s) \\ 0 = R_s \psi_{sq-}^- (s) / L'_s + \omega_2 \psi_{sd-}^- (s) + s \psi_{sq-}^- (s) \end{cases} \quad (32)$$

where U_{sn} is the amplitude of the stator voltage vector under normal conditions and $L'_s = L_s - L_m^2 / L_r$.

According to the Equations (28) and (31), taking the d -axis component of the stator flux in the $(dq)^+$ reference frame, for example, it can be expressed as:

$$\psi_{sd+}^+ (s) = -N(s) \cdot \frac{s + R_s / L'_s}{(s + R_s / L'_s)^2 + \omega_1^2} \cdot \frac{U_{s+}}{s} - \frac{(s + R_s / L'_s) \cdot U_{s-}}{s D_{sd+}^+ (s)} - \frac{U_{sn}}{\omega_1} \cdot \frac{\omega_1}{(s + R_s / L'_s)^2 + \omega_1^2} \quad (33)$$

where $D_{sd+}^+ (s) = [(s + R_s / L'_s)^2 + \omega_1^2] \cdot (s^2 + 2\varepsilon\omega_n s + \omega_n^2)$. Assuming the $D_{sd+}^+ (s)$ is equal to 0, the closed-loop poles can be obtained such that:

$$\begin{cases} s_{1,2} = -R_s / L'_s \pm j\omega_1 \\ s_{3,4} = -\varepsilon\omega_n \pm j\sqrt{1 - \varepsilon^2} \omega_n \end{cases} \quad (34)$$

where $\varepsilon\omega_n$ is much greater than R_s / L'_s . Hence, the $s_{1,2}$ is the dominant pole of the transfer function $D_{sd+}^+ (s)$. Meanwhile, the amplitude of $|(s + R_s / L'_s) / s D_{sd+}^+ (s_{1,2})|$ is so small that the influence of negative-sequence voltage can be neglected. Therefore, the closed-loop transfer function represented in the form for the d -axis component of the stator flux in the $(dq)^+$ reference frame during the fault transient period can be rewritten as:

$$\begin{aligned} \psi_{sd+}^+ (s) &= -\frac{U_{sn}}{\omega_1} \cdot \frac{\omega_1}{(s + R_s / L'_s)^2 + \omega_1^2} + N(s) \cdot \frac{s + R_s / L'_s}{(s + R_s / L'_s)^2 + \omega_1^2} \cdot \frac{U_{s+}}{s} \\ &= -\frac{U_{sn}}{\omega_1} \cdot \frac{\omega_1}{(s + R_s / L'_s)^2 + \omega_1^2} + U_{s+} \cdot \left(\frac{A_d}{s} + \frac{A_1 s + B_1}{(s + R_s / L'_s)^2 + \omega_1^2} + \frac{A_2 s + B_2}{s^2 + 2\varepsilon\omega_n s + \omega_n^2} \right) \end{aligned} \quad (35)$$

The expression for the coefficients $A_d, A_1, A_2, B_1,$ and B_2 can be found in Appendix A.

Likewise, expression as shown in Equation (36) can be obtained:

$$\psi_{sq+}^+ (s) = -\frac{U_{sn}}{\omega_1} \cdot \frac{s + R_s / L'_s}{(s + R_s / L'_s)^2 + \omega_1^2} - \frac{U_{s+}}{\omega_1} \cdot \left(\frac{A_q}{s} + \frac{A_3 s + B_3}{(s + R_s / L'_s)^2 + \omega_1^2} + \frac{A_4 s + B_4}{s^2 + 2\varepsilon\omega_n s + \omega_n^2} \right) \quad (36)$$

The expression for the coefficients $A_q, A_3, A_4, B_3,$ and B_4 can be found in Appendix B.

Since one of the damping time constants $\tau_2 = 1 / \varepsilon\omega_n \approx 2.25ms$, this means that the transient period is approximately 10.0 ms, which can be neglected. Meanwhile, the term R_s / L'_s is so small compared with the terms $\varepsilon\omega_n$ and ω_n^2 . Hence, the term R_s / L'_s can be neglected. Under this condition, the approximate value of the terms $A_d, A_1, B_1, A_q, A_3,$ and B_3 can be obtained. Accordingly, $A_d \approx 0, A_1 \approx -6\sqrt{2} / 17\omega_1, B_1 \approx 9 / 17,$ and $A_q \approx 1, A_3 \approx -9 / 17,$ and $B_3 \approx -6\sqrt{2}\omega_1 / 17$. Based on this, the d -axis and q -axis components of the stator flux in the $(dq)^+$ reference frame can be expressed as:

$$\begin{cases} \psi_{sd+}^+ = -K_+ e^{-R_s t / L'_s} \sin(\omega_1 t + \theta_1) \\ \psi_{sq+}^+ = -U_{s+} / \omega_1 - K_+ e^{-R_s t / L'_s} \cos(\omega_1 t + \theta_1) \end{cases} \quad (37)$$

with $K_+ = \sqrt{(9U_{s+} - 17U_{sn})^2 + 72U_{s+}^2} / (17\omega_1)$ and $\theta_1 = \arctan[6\sqrt{2}U_{s+} / (17U_{sn} - 9U_{s+})]$.

Likewise, the expressions of the d -axis and q -axis components of the stator flux linkages in the $(dq)^-$ reference frame can be obtained:

$$\begin{cases} \psi_{sd-}^- = -K_- e^{-R_{st}/L_s} \sin(\omega_1 t + \theta_2) \\ \psi_{sq-}^- = U_{s-} / \omega_1 + K_- e^{-R_{st}/L_s} \cos(\omega_1 t + \theta_2) \end{cases} \quad (38)$$

with $K_- = 3U_{s-} / (\sqrt{17} \omega_1)$ and $\theta_2 = \arctan(2\sqrt{2}/3)$.

5. Fault Current Characteristics of the Doubly-Fed Induction Generator (DFIG)

By substituting the expression of stator flux linkages (ψ_{sd+}^+ , ψ_{sq+}^+ , ψ_{sd-}^- , and ψ_{sq-}^-) and the expression of rotor currents (i_{rd+}^+ , i_{rq+}^+ , i_{rd-}^- , and i_{rq-}^-) into the equations of Equation (2), the time domain expressions of the d -axis and q -axis components of the stator current in the $(dq)^+$ and $(dq)^-$ reference frames can be obtained as follows:

$$\begin{cases} i_{sd+}^+(t) = L_m i_{rd+}^{*+} / L_s + K_+ (L_m K_d + 1) \cdot e^{-R_{st}/L_s} \sin(\omega_1 t + \theta_1) / L_s \\ i_{sq+}^+(t) = (\omega_1 L_m i_{rq+}^{*+} + U_{s+}) / \omega_1 L_s + K_+ (L_m K_d + 1) \cdot e^{-R_{st}/L_s} \cos(\omega_1 t + \theta_1) / L_s \end{cases} \quad (39)$$

$$\begin{cases} i_{sd-}^-(t) = L_m i_{rd-}^{*-} / L_s + K_- (L_m K_d + 1) \cdot e^{-R_{st}/L_s} \sin(\omega_1 t + \theta_2) / L_s \\ i_{sq-}^-(t) = (\omega_1 L_m i_{rq-}^{*-} - U_{s-}) / \omega_1 L_s - K_- (L_m K_d + 1) \cdot e^{-R_{st}/L_s} \cos(\omega_1 t + \theta_2) / L_s \end{cases} \quad (40)$$

The coordinate transformation is applied to Equation (39), the positive-sequence components of three-phase stator fault currents can be derived as:

$$\begin{cases} i_{sa+}(t) = I_{1+} \cos(\omega_1 t + \theta_{a1} + \gamma_{1+}) + K_+ (L_m K_d + 1) e^{-R_{st}/L_s} \sin(\theta_1 - \theta_{a1}) / L_s \\ i_{sb+}(t) = I_{1+} \cos(\omega_1 t + \theta_{b1} + \gamma_{1+}) + K_+ (L_m K_d + 1) e^{-R_{st}/L_s} \sin(\theta_1 - \theta_{b1}) / L_s \\ i_{sc+}(t) = I_{1+} \cos(\omega_1 t + \theta_{c1} + \gamma_{1+}) + K_+ (L_m K_d + 1) e^{-R_{st}/L_s} \sin(\theta_1 - \theta_{c1}) / L_s \end{cases} \quad (41)$$

where $\theta_{a1} = \theta_0$, $\theta_{b1} = \theta_0 - 2\pi/3$, $\theta_{c1} = \theta_0 + 2\pi/3$, and θ_0 is the angle between the stator voltage vector and stator current vector at the moment that the fault occurs. Meanwhile, $I_{1+} = \sqrt{(\omega_1 L_m i_{rd+}^{*+})^2 + (\omega_1 L_m i_{rq+}^{*+} + U_{s+})^2} / (\omega_1 L_s)$ and $\gamma_{1+} = \arctan[(\omega_1 L_m i_{rq+}^{*+} + U_{s+}) / \omega_1 L_m i_{rd+}^{*+}]$.

Likewise, the negative-sequence components of three-phase stator currents can be derived as:

$$\begin{cases} i_{sa-}(t) = I_{1-} \cos(\omega_1 t + \theta_{a2} + \gamma_{1-}) + K_- (L_m K_d + 1) e^{-R_{st}/L_s} \sin(\theta_2 + \theta_{a2}) / L_s \\ i_{sb-}(t) = I_{1-} \cos(\omega_1 t + \theta_{b2} + \gamma_{1-}) + K_- (L_m K_d + 1) e^{-R_{st}/L_s} \sin(\theta_2 + \theta_{b2}) / L_s \\ i_{sc-}(t) = I_{1-} \cos(\omega_1 t + \theta_{c2} + \gamma_{1-}) + K_- (L_m K_d + 1) e^{-R_{st}/L_s} \sin(\theta_2 + \theta_{c2}) / L_s \end{cases} \quad (42)$$

where $\theta_{a2} = \theta_0$, $\theta_{b2} = \theta_0 + 2\pi/3$, $\theta_{c2} = \theta_0 - 2\pi/3$. Meanwhile, $I_{1-} = \sqrt{(\omega_1 L_m i_{rd-}^{*-})^2 + (\omega_1 L_m i_{rq-}^{*-} - U_{s-})^2} / (\omega_1 L_s)$ and $\gamma_{1-} = \arctan[(\omega_1 L_m i_{rq-}^{*-} - U_{s-}) / \omega_1 L_m i_{rd-}^{*-}]$.

Accordingly:

$$\begin{cases} i_{sa}(t) = i_{sa+}(t) + i_{sa-}(t) \\ i_{sb}(t) = i_{sb+}(t) + i_{sb-}(t) \\ i_{sc}(t) = i_{sc+}(t) + i_{sc-}(t) \end{cases} \quad (43)$$

6. Simulation Study

Under unbalanced fault conditions, there are various control strategies available for the LVRT requirement of the DFIG [26–33]. Therefore, the effect of the control strategy on the fault current characteristics of the DFIG must be considered.

6.1. Heading Steady-state Reference Signals of Rotor Current

In this paper, in order to ensure balanced heating on the three-phase stator winding, the control target for balanced stator current of the DFIG is used [28]. Therefore, under stable operating condition:

$$\bar{i}_{sd-} = 0, \bar{i}_{sq-} = 0 \tag{44}$$

Moreover, in order to provide sufficient reactive current to meet the requirements of the grid code [6], the reactive current reference signal denoted by I_r during grid fault should be:

$$I_r = \begin{cases} 0 & \lambda > 0.9 \\ 2 \cdot (0.9 - \lambda) & 0.2 \leq \lambda \leq 0.9 \end{cases} \tag{45}$$

where all parameters are given in per unit system, and λ represents the magnitude of the positive-sequence grid voltage after a fault occurs. Due to the q -axis component of the stator current in the $(dq)^-$ reference frame being zero, the q -axis component of the stator current in the $(dq)^+$ reference frame under stable operating condition can be expressed as:

$$\bar{i}_{sq+}^+ = -2 \cdot (0.9 - u_{sd+}^+) \tag{46}$$

In addition, to ensure the safety of the RSC, the maximum rotor current I_{rset} , which is within the admissible overload capability of the RSC, should also be provided. The typical value of I_{rset} is 1.2 per unit (p.u.) [29].

By substituting Equations (44) and (46) into the Equations (1)–(4), the steady-state reference signals of the rotor current in the $(dq)^+$ and $(dq)^-$ references frame under unbalanced fault conditions can be expressed as follows:

$$\begin{cases} \bar{i}_{rdf+}^{**} = \sqrt{I_{rset}^2 - \bar{i}_{rjf+}^{**2} - \bar{i}_{rdf-}^{**2} - \bar{i}_{rjf-}^{**2}} \\ \bar{i}_{rjf+}^{**} = -u_{sd+}^+ / \omega_1 L_m - 2L_s (0.9 - u_{sd+}^+) / L_m \\ \bar{i}_{rdf-}^{**} = 0 \\ \bar{i}_{rjf-}^{**} = u_{sd-}^- / \omega_1 L_m \end{cases} \tag{47}$$

According to Equation (47), on condition that the control target for “balanced stator current” is applied in the DFIG, the expressions of the positive- and negative-sequence components of the three-phase stator fault currents can be obtained.

6.2. Simulation Analysis

In order to validate the previous theoretical analysis results, a simulation model with the DFIG is built in the PSCAD/EMTDC software environment. Among them, the simulation model of the DFIG’s control system is derived from reference [17] and the control target for balanced stator current of the DFIG is derived from reference [26].

It should be noted that the improved control strategy of the GSC presented is adopted to limit the fluctuation of the DC-link voltage [31]. Additionally, the rotate speed is kept constant during grid faults.

The details of the 10.5 kV, 50 Hz test system shown in Figure 5 are as follows. In Figure 5, the line parameters are $r(1) = r(2) = 0.27 \Omega/\text{km}$ and $x(1) = x(2) = 0.494 \Omega/\text{km}$. The Zero sequence parameter of the line are $r(0) = 0.29 \Omega/\text{km}$ and $x(0) = 0.53 \Omega/\text{km}$. The total length of line L is 25 km. The rated capacity of the T is 2.5/2.5 MVA, the turn ratio is 0.69 kV/10.5 kV, the winding type is Y/D , and the leakage reactance is 0.0622 p.u. The voltage magnitude (L-L) of the synchronous generator G is 10.5 kV, the phase angle is 0° , and the internal resistance is 0.5Ω .

The parameters of the 1.5-MW rated DFIG are:

$U_{sn} = 690\text{V}$, $f_n = 50\text{Hz}$, $L_s = L_r = 2.3192\text{p.u.}$, $L_m = 2.1767\text{p.u.}$, $R_s = 0.00756\text{p.u.}$, $R_r = 0.00533\text{p.u.}$, $\omega_c = 7\omega_1$, $p = 2$, $n_{max} = 1800\text{r/min}$.

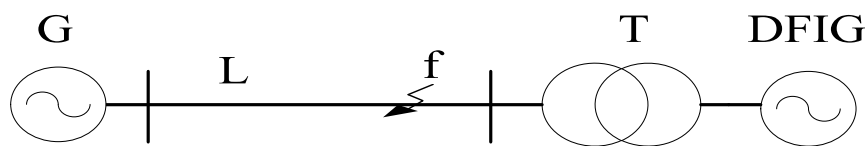


Figure 5. Test system of the DFIG.

For the following simulation examples, the output active power of the DFIG is 1.0 p.u. and the grid voltage is 1.0 p.u. before the fault occurs. The fault current characteristics of the DFIG are studied in a variety of fault conditions, including different fault types and fault points. Among them, the fault happens to be 5 km away from the DFIG in the line L at time $t = 5.0$ s and results in Phase-C ground fault that has been used for the simulation example. Under this fault condition, the positive-and negative-sequence components of the stator voltage are 0.57 p.u. and 0.215 p.u., respectively.

6.2.1. Stator Flux Linkage

Figure 6 shows the simulation results of the d -axis and q -axis components of the stator flux linkage (ψ_{sd+}^+ , ψ_{sq+}^+ , ψ_{sd-}^- and ψ_{sq-}^-) in the $(dq)^+$ and $(dq)^-$ reference frames. In Figure 6, Y represents the flux linkage. “pp” and “nn” represent the positive-and negative-sequence components, respectively. The “-ap” represents the simulation results. Another waveform represents the theoretical analysis result. Notice that all values in the theoretical analysis results and simulation results are the per-unit value (p.u.).

It can be observed that there are damped fundamental frequency components in the q -axis and d -axis components of the stator flux linkage in the $(dq)^+$ and $(dq)^-$ reference frames. Meanwhile, there are no DC components in ψ_{sd+}^+ and ψ_{sd-}^- . However, there are DC components in ψ_{sq+}^+ and ψ_{sq-}^- , whose amplitudes are approximately proportional to the amplitude of positive-and negative-sequence components of the grid voltage, respectively.

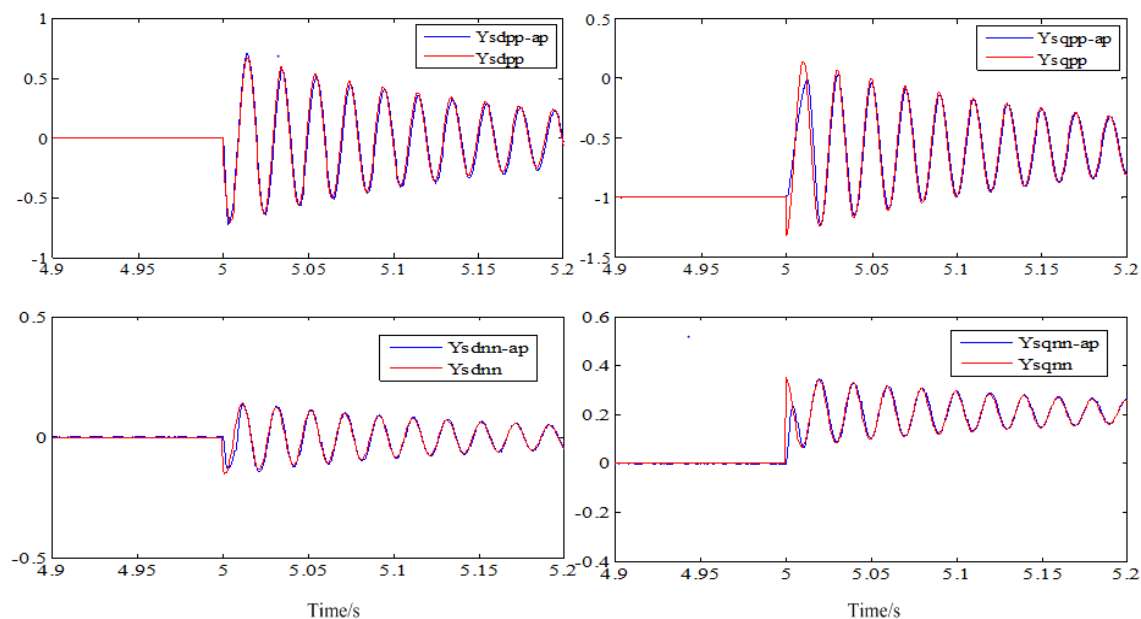


Figure 6. *d*-axis and *q*-axis components of the stator flux linkage in the $(dq)^+$ and $(dq)^-$ reference frames.

6.2.2. Rotor Current and Stator Current

Figure 7 shows the comparisons between the theoretical analysis results and simulation results of the *d*-axis and *q*-axis components of the rotor current in the $(dq)^+$ and $(dq)^-$ reference frames.

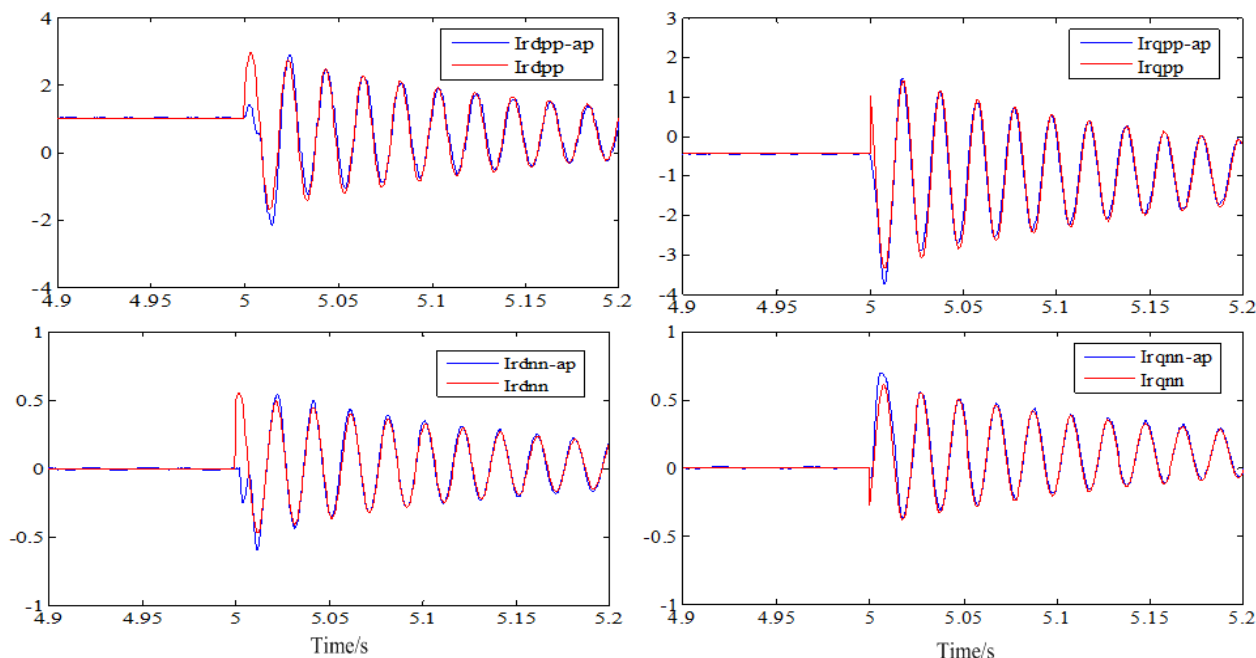


Figure 7. *d*-axis and *q*-axis components of the rotor current in the $(dq)^+$ and $(dq)^-$ reference frames.

It can be seen from Figure 7 that the differences between the simulation results and theoretical analysis results of the rotor currents are very small. When the control target for the balanced stator current is applied in the DFIG, there are damped fundamental frequency components and DC components in the rotor currents (i_{rd+}^+ , i_{rq+}^+ , and i_{rq-}^-), but only damped fundamental frequency

components in the d -axis fault component of the rotor current i_{rd}^- in the $(dq)^-$ reference frame. Additionally, the amplitude of the DC component is not damped.

In addition, it can be seen in Figure 7 that there is a small deviation from the calculated rotor currents at initial conditions (about 1/2 cycle after fault initiation) and the simulated rotor currents. This is due to the derivation of the analytical expression for rotor currents being based on the assumed condition that the voltage fluctuations during the grid fault conditions are neglected. In fact, when a fault occurs in the line L, there are oscillations in the terminal voltages of the DFIG due to the imbalance of the instantaneous power during the initial stage. This is the reason why the initial conditions of the calculated rotor currents are different for the simulated rotor currents.

Figure 8 shows the comparisons between the theoretical analysis results and simulation results of the d -axis and q -axis components of the stator currents in the $(dq)^+$ and $(dq)^-$ reference frames.

Figure 9 illustrates the amplitude of the positive- and negative-sequence fundamental frequency components of the stator currents ($AMP_{I_{sa1pp}}$ and $AMP_{I_{sa1nn}}$), the phase angle of positive-sequence fundamental frequency component ($PH_{I_{sa1pp}}$), and the damped DC component ($AMP_{I_{sa dc}}$).

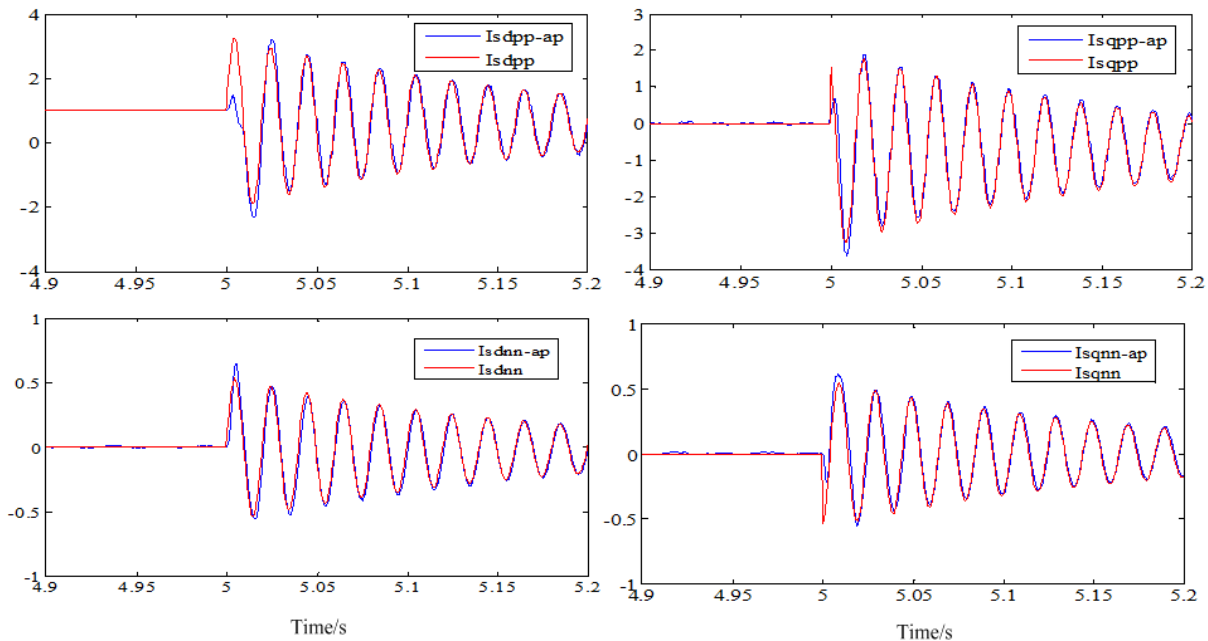


Figure 8. d -axis and q -axis components of the stator current in the $(dq)^+$ and $(dq)^-$ reference frames.

It can be observed from Figure 8 and Figure 9 that there are damped DC components and steady-state fundamental frequency components in the positive-sequence components of the stator currents (i_{sd}^+ and i_{sq}^+). The amplitude and phase angle of the positive-sequence fundamental frequency components in the stator currents are related to the corresponding control target of the DFIG and the amplitude of the positive-sequence stator voltage component. The amplitude of the damped DC component is not only related to the corresponding control target of the DFIG and the amplitude of the positive-sequence stator voltage component, but also affected by the phase angle of the pre-fault current and the amplitude of the negative-sequence stator voltage component.

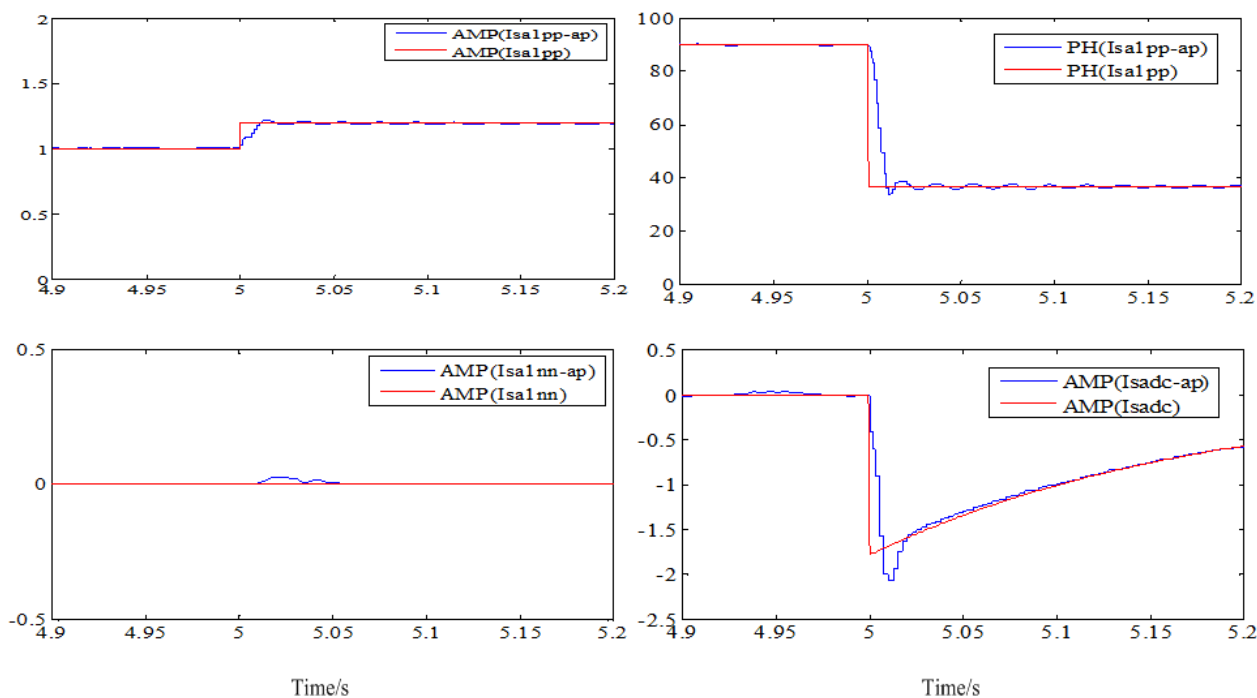


Figure 9. The A phase current under condition of a Phase-C ground fault.

The composition of the negative-sequence stator current components is related to the control target of the DFIG. When the control target for the balanced stator current is applied in the DFIG, there is only a damped fundamental frequency component and without the DC component in the negative-sequence stator current components (i_{sd-}^- and i_{sq-}^-). However, there is not only the DC component, but also the damped fundamental frequency components of the negative-sequence stator current components in the $(dq)^-$ reference frame on the condition that the “constant electromagnetic torque” or “balanced rotor current” of the control target is applied in the DFIG [28]. In addition, it can be seen from Figure 8 that the amplitude of the damped fundamental frequency component is only related to the amplitude of the negative-sequence stator voltage component. However, the initial phase angle of the damped fundamental frequency component is constant and it is independent of the negative-sequence stator voltage component. Moreover, the amplitude of the damped fundamental frequency component is proportional to the amplitude of the negative-sequence stator voltage component.

In Figure 10, the simulation results of the Phase-C stator current on the different conditions, of the DFIG without the notch filters (I_{sc-ap1}) and with the notch filters (I_{sc-ap}), and the theoretical analysis results of the Phase-C stator current on the condition that the DFIG with the notch filters (I_{sc}), are compared. Due to lack of space, only the comparison of the stator current (with or without notch filters) has been shown in this paper. In fact, the AC components with frequency of $2\omega_1$ exist in the stator flux linkages, the rotor currents, the stator currents, and the stator voltages on the DFIG, which the phase angles cannot be an accurate estimation by the conventional PLL techniques and without the notch filters.

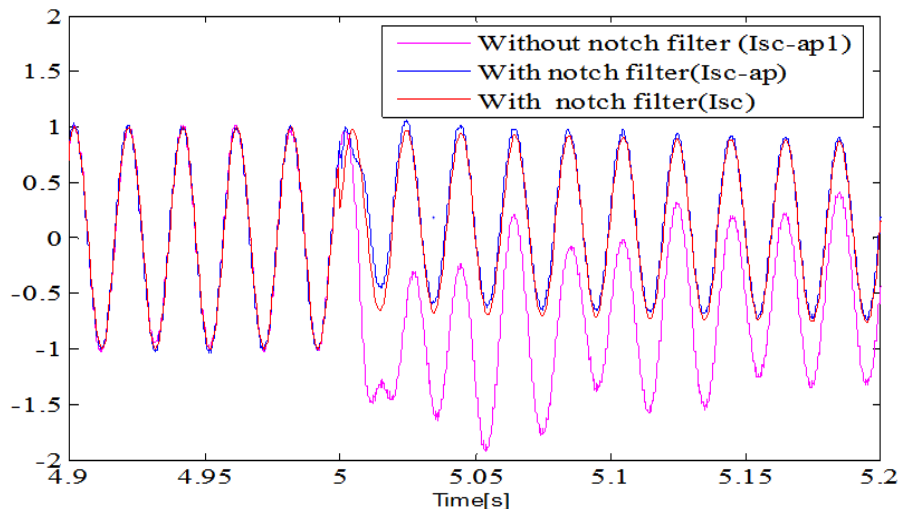


Figure 10. The C phase currents under condition of a Phase-C ground fault.

It can be observed from the Figure 10 that the AC components with frequency of 2ω , in the stator current has been eliminated by the notch filters and there exist the AC components with a frequency of 2ω , in the stator current without the notch filters. Moreover, the difference between the simulation result and theoretical analysis result of the Phase-C current is very small, which validate the effectiveness of the theoretical analysis.

In addition, there are only damped DC components and steady-state fundamental frequency components in the stator currents based on the aforementioned analysis. For the fundamental frequency components, there are non-linear relationships between the fault voltage and the fault current of the DFIG. Hence, on the condition that the control target for “balanced stator current” is applied in the DFIG, the DFIG can be represented by a controlled positive-sequence current source. On the condition that the control target for “balanced rotor current” or “constant electromagnetic torque” is applied in the DFIG, the DFIG can be represented by a controlled positive-sequence current source and a controlled negative-sequence current source.

7. Conclusions

The fault current characteristics of the DFIG are studied in this paper on condition that an unbalanced fault occurs and the rotor windings are excited by the AC/DC/AC converter. Under unbalanced fault conditions, the electrical variables oscillate at twice the grid frequency in the synchronous dq frame. In the engineering practice, notch filters are usually used to extract the positive and negative sequence components in the synchronous dq frame. Hence, the notch filters have a large influence on the fault current characteristics of the DFIG. In this paper, the dynamic performance of the stator flux linkage and the rotor current are analyzed. Based on this, the stator fault current characteristics of the DFIG under unbalanced fault conditions are studied. This study is of great significance for safe and stable operation of the power grid with penetration of DFIGs. The obtained conclusions can be drawn as follows:

(1) The amplitude and phase angle of the stator flux linkage in the DFIG are changed by the notch filters. Moreover, the range of the PI parameters and the dynamic performance of the RSC are also influenced by the notch filters.

(2) The transient behaviors of the DFIG are analyzed, and simple expressions of the DFIG transient electrical variables are proposed. The acquired transient characteristics provide good references to improve DFIG control during unbalanced grid faults.

(3) Under unbalanced fault conditions, the stator fault current characteristics of the DFIG are different from those of a conventional synchronous generator. There is only a damped DC component and steady-state fundamental frequency component in the stator fault current. The amplitude of the damped DC component of the stator fault current is related to the depth of the grid voltage dip and the phase angle of the pre-fault current. The steady-state fundamental frequency component is not only related to the depth of the grid voltage dip, but also affected by the corresponding control target of the DFIG.

(4) For the fundamental frequency component, on the condition that the control target for “balanced stator current” is applied in the DFIG, the DFIG can be represented by a controlled positive-sequence current source. On the condition that the control target for “balanced rotor current” or “constant electromagnetic torque” is applied in the DFIG, the DFIG can be represented by a controlled positive-sequence current source and a controlled negative-sequence current source. This is helpful to meet the requirements of a practical short-circuit calculation and the construction of a relaying protection system for the power grid with penetration of DFIGs.

Acknowledgments

This work was supported by the National Natural Science Foundation of China (No. 51177058 and No. 51277084).

Author Contributions

Fan Xiao and Zhe Zhang designed the model and the experiments. Fan Xiao carried out the experiments. Fan Xiao and Xianggen Yin analyzed and interpreted data. Fan Xiao, Zhe Zhang and Xianggen Yin concluded the scientific findings and prepared the manuscript.

Conflicts of Interest

The authors declare no conflict of interest.

Appendix A

$$A_1 = \frac{\frac{K_2 - (R_s^2/L_s^2 + \omega_1^2)K_1 - 2\varepsilon K_3/\omega_n}{2R_s/L_s' - 2\varepsilon(R_s^2/L_s'^2 + \omega_1^2)/\omega_n} - \frac{(K_4 - 2R_s K_1/L_s' - K_3/\omega_n^2) \omega_n^2}{\omega_n^2 - \omega_1^2 - R_s^2/L_s'^2}}{\frac{(2R_s/L_s' - 2\varepsilon\omega_n) \cdot \omega_n^2}{\omega_n^2 - \omega_1^2 - R_s^2/L_s'^2} + \frac{\omega_n^2 - \omega_1^2 - R_s^2/L_s'^2}{2R_s/L_s' - 2\varepsilon(R_s^2/L_s'^2 + \omega_1^2)/\omega_n}} \quad (48)$$

$$A_u = \frac{R_s/L_s'}{R_s^2/L_s'^2 + \omega_1^2} \quad (49)$$

$$B_1 = \frac{K_3}{\omega_n^2} - B_2 \cdot \frac{R_s^2/L_s'^2 + \omega_1^2}{\omega_n^2} \quad (50)$$

$$A_2 = K_1 - A_1 \quad (51)$$

$$B_2 = \frac{K_2 - (R_s^2/L_s^e + \omega_1^2)K_1 - 2\varepsilon K_3/\omega_n}{2R_s/L_s' - 2\varepsilon(R_s^2/L_s^e + \omega_1^2)/\omega_n} + A_1 \frac{\omega_1^2 + R_s^2/L_s^e - \omega_n^2}{2R_s/L_s' - 2\varepsilon(R_s^2/L_s^e + \omega_1^2)/\omega_n} \quad (52)$$

$$K_1 = -\frac{R_s/L_s'}{R_s^2/L_s^e + \omega_1^2} \quad (53)$$

$$K_2 = R_s/L_s' - (\omega_n^2 + 4\varepsilon\omega_n R_s/L_s' + R_s^2/L_s^e + \omega_1^2)A_d \quad (54)$$

$$K_3 = \omega_n^2 - 2\omega_n^2 A_d R_s/L_s^e + 2\varepsilon\omega_n A_d (\omega_1^2 + R_s^2/L_s^e) \quad (55)$$

$$K_4 = 1 - (2R_s/L_s^e + 2\varepsilon\omega_n)A_d \quad (56)$$

Appendix B

$$A_3 = \frac{\frac{K_7 - (R_s^2/L_s^e + \omega_1^2)/K_5 - 2\varepsilon K_8/\omega_n}{2R_s\omega_n^2/L_s' - 2\varepsilon\omega_n(R_s^2/L_s^e + \omega_1^2)} - \frac{K_6 - 2R_s K_5/L_s' - K_8/\omega_n^2}{\omega_n^2 - \omega_1^2 - R_s^2/L_s^e}}{\frac{2R_s/L_s' - 2\varepsilon\omega_n}{\omega_n^2 - \omega_1^2 - R_s^2/L_s^e} + \frac{\omega_n^2 - \omega_1^2 - R_s^2/L_s^e}{2R_s\omega_n^2/L_s' - 2\varepsilon\omega_n(R_s^2/L_s^e + \omega_1^2)}} \quad (57)$$

$$A_4 = \frac{\omega_1^2}{R_s^2/L_s^e + \omega_1^2} \quad (58)$$

$$B_3 = \frac{K_8}{\omega_n^2} - B_4 \cdot \frac{R_s^2/L_s^e + \omega_1^2}{\omega_n^2} \quad (59)$$

$$A_4 = K_5 - A_3 \quad (60)$$

$$B_4 = \frac{K_6 - 2K_5 R_s/L_s' - K_8/\omega_n^2}{\omega_n^2 - \omega_1^2 - R_s^2/L_s^e} \cdot \omega_n^2 + A_3 \omega_n^2 \cdot \frac{2R_s/L_s' - 2\varepsilon\omega_n}{\omega_n^2 - \omega_1^2 - R_s^2/L_s^e} \quad (61)$$

$$K_5 = -\frac{\omega_1^2}{R_s^2/L_s^e + \omega_1^2} \quad (62)$$

$$K_6 = -(R_s/L_s^e + 2\varepsilon\omega_n)A_q \quad (63)$$

$$K_7 = \omega_1^2 - A_q \omega_n^2 - 4\varepsilon\omega_n A_q R_s/L_s' - (\omega_1^2 + R_s^2/L_s^e)A_q \quad (64)$$

$$K_8 = -[2R_s\omega_n^2/L_s' + 2\varepsilon\omega_n(R_s^2/L_s^e + \omega_1^2)]A_q \quad (65)$$

References

1. Muller, S.; Deicke, M.; de Doncker, R.W. Doubly fed induction generator systems for wind turbines. *IEEE Ind. Appl. Mag.* **2002**, *8*, 26–33.
2. Iwanski, G.; Koczara, W. DFIG-based power generation system with UPS function for variable-speed applications. *IEEE Trans. Ind. Electron.* **2008**, *55*, 3047–3054.
3. Jauch, C.; Matevosyan, J.; Ackermann, T.; Bolik, S. International comparison of requirements for connection of wind turbines to power systems. *Wind Energy* **2005**, *8*, 295–306.
4. The grid Code 3. Available online: <http://www.nationalgrid.com/uk/Electricity/Codes/gridcode> (accessed on 1 January 2006).

5. Transmission Code 2007—Network and System Rules of the German Transmission System Operators. Available online: <https://www.bdew.de/> (accessed on 1 August 2007).
6. *Technical Rule for Connecting Wind Farm to Power System*; Technical Report for Inspection and Quarantine of the People's Republic of China: Beijing, China, 2011.
7. Howard, D.F.; Habetler, T.G.; Harley, R.G. Improved sequence network model of wind turbine generators for short-circuit studies. *IEEE Trans. Energy Convers.* **2012**, *27*, 968–977.
8. Morren, J.; de Haan, S.W.H. Ridethrough of wind turbines with doubly-fed induction generator during a voltage dip. *IEEE Trans. Energy Convers.* **2005**, *20*, 435–441.
9. Lopez, J.; Sanchis, P.; Roboam, X.; Marroyo, L. Dynamic behavior of the doubly-fed induction generator during three-phase voltage dips. *IEEE Trans. Energy Convers.* **2007**, *22*, 709–717.
10. Morren, J.; de Haan, S.W. Short-circuit current of wind turbines with doubly fed induction generator. *IEEE Trans. Energy Convers.* **2007**, *22*, 174–180.
11. Pannell, G.; Atkinson, D.J.; Zahawi, B. Analytical study of grid-fault response of wind turbine doubly fed induction generator. *IEEE Trans. Energy Convers.* **2010**, *25*, 1081–1091.
12. Zhang, L.H.; Cai, X.; Guo, J.H. Dynamic response of DFIG fault currents under constant AC excitation condition. In Proceedings of the 2009 Asia-Pacific Power Energy Engineering Conference (APPEEC), Wuhan, China, 27–31 March 2009; pp. 1–4.
13. Wu, Z.R.; Wang, G.; Li, H.F.; Gao, X. Equivalent Model for Calculating Short Circuit Current of Doubly Fed Wind Generator under Uninterrupted Excitation. In Proceedings of the 2011 Power Energy Engineering Conference (APPEEC), Wuhan, China, 25–28 March 2011; pp. 1–4.
14. Kong, X.; Zhang, Z.; Yin, X. Study of Fault Current Characteristics of the DFIG Considering Dynamic Response of the RSC. *IEEE Trans. Energy Convers.* **2014**, *29*, 278–287.
15. Ouyang, J.; Xiong, X. Dynamic behavior of the excitation circuit of a doubly-fed induction generator under a symmetrical voltage drop. *Renew. Energy* **2014**, *71*, 629–638.
16. Timbus, V.; Ciobotaru, M.; Teodorescu, R.; Blaabjerg, F. Adaptive Resonant Controller for Grid-Connected Converters in Distributed Power Generation Systems. In Proceedings of the Twenty-First Annual IEEE Applied Power Electronics Conference and Exposition (APEC), Dallas, TX, USA, 26–30 March 2006; pp. 1601–1606.
17. Nian, H.; Song, Y.; Zhou, P.; He, Y. Improved direct power control of a wind turbine driven doubly fed induction generator during transient grid voltage unbalance. *IEEE Trans. Energy Convers.* **2011**, *26*, 976–986.
18. Yazdani, D.; Bakhshai, A.; Joos, G. A Real-Time Sequence Components Decomposition for Transient Analysis in Grid-Connected Distributed Generation Systems. In Proceedings of the IEEE International Symposium on Industrial Electronics (ISIE), Cambridge, UK, 30 June–2 July 2008; pp. 1651–1656.
19. Leonhard, W. *Control of Electrical Drives*; Springer-Verlag: Berlin, Germany, 1995.
20. Marques, G.D.; Sousa, D.M. Understanding the doubly fed induction generator during voltage dips. *IEEE Trans. Energy Convers.* **2012**, *27*, 421–461.
21. Hopfensperger, B.; Atkinson, D.J. Stator-flux-oriented control of a doubly-fed induction machine with and without position encoder. *IEE Proc. Electr. Power Appl.* **2000**, *147*, 241–250.
22. Wang, L.; Zhu, H.; Yang, Z. Tuning Method for PI Controllers of PMSM Driving System. *Trans. China Electrotech. Soc.* **2014**, *5*, 104–117.

23. Lopez, J.; Gubia, E.; Olea, E.; Ruiz, J.; Marroyo, L. Ride through of wind turbines with doubly fed induction generator under symmetrical voltage dips. *IEEE Trans. Ind. Electron.* **2009**, *56*, 4246–4254.
24. Liu, Q.H.; He, Y.K.; Zhang, J.H. Operation control and modeling simulation of AC-excited variable-speed constant-frequency wind power generator. *Proc. CSEE* **2006**, *26*, 43–50.
25. Jia, J.C.; Liu, J.; Zhang, Y.G. Dynamic characteristics of stator flux of doubly-fed induction generator during grid voltage fault. *Proc. CSEE* **2011**, *31*, 90–96.
26. Lie, X.; Yi, W. Dynamic modeling and control of DFIG based wind turbines under unbalanced network conditions. *IEEE Trans. Power Syst.* **2007**, *22*, 314–323.
27. Hu, J. Investigation on the Ride-Through Operation of DFIG-based Wind Power Generation Systems during Grid Fault-Basic Theory and Key Technology. Ph.D. Thesis, Zhejiang University, Hangzhou, China, 2009.
28. Zheng, Z.; Yang, G.; Geng, H. Coordinated control of a doubly-fed induction generator-based wind farm and a static synchronous compensator for low voltage ride-through grid code compliance during asymmetrical grid faults. *Energies* **2013**, *6*, 4660–4681.
29. Wang, Y.; Wu, Q.; Xu, H.; Guo, Q.; Sun, H. Fast coordinated control of DFIG wind turbine generators for low and high voltage ride-through. *Energies* **2014**, *7*, 4140–4156.
30. Wu, Z.; Zhu, C.; Hu, M. Improved control strategy for DFIG wind turbines for low voltage ride through. *Energies* **2013**, *6*, 1181–1197.
31. Yao, J.; Li, H.; Liao, Y.; Chen, Z. An improved control strategy of limiting the dc-link voltage fluctuation for a doubly fed induction wind generator. *IEEE Trans. Power Electron.* **2008**, *23*, 1205–1213.
32. Papadimitriou, C.N.; Vovos, N.A. Transient response improvement of microgrids exploiting the inertia of a Doubly-Fed Induction Generator (DFIG). *Energies* **2010**, *3*, 1049–1066.
33. Arribas, J.R.; Rodríguez, A.F.; Muñoz, Á.H.; Nicolás, C.V. Low voltage ride-through in DFIG wind generators by controlling the rotor current without crowbars. *Energies* **2014**, *7*, 498–519.